AN ABSTRACT OF THE THESIS OF

Donald A. Schneider for the degree of Master of Science in Mechanical Engineering presented on August 18, 1998. Title: Thermal Contact Resistances in a Thermal Conductivity Test System.

Redacted for Privacy

Abstract Approved: _____

Ernest G. Wolff

The thermal contact conductance (TCC) between two machined pieces of stainless steel was studied. A guarded hot plate thermal conductivity test fixture was designed and built for the experiment. Factors investigated included the contact pressure, surface roughness, interface material and average test temperature. The contact pressure at the interface ranged from 80 to 800 psi. The mean surface roughness of the opposing surfaces was 2.8 μin (.0708 μm) parallel to the sanding direction and 1.9 μin (.0482 μm) perpendicular to the sanding direction. Interface materials included air, indium foil, copper foil, Teflon tape, silver filled paint and thermal grease. Average test temperatures ranged from 0 °C to 100 °C, in 20 °C increments.

With air alone in the interface gap the TCC was nearly insensitive to contact pressure. The thermal grease and silver filled paint most increased the TCC over air alone while being nearly insensitive to pressure. With indium foil the TCC was similar to air, but improved somewhat with increasing pressure. With copper foil the TCC was lower than air alone, but increased with increasing pressure. The Teflon tape had a lower TCC than air at low contact pressure, but a higher TCC than air at higher pressures. In general the TCC improved somewhat at higher temperatures. The ability of an interface material to improve the TCC is more a function of its flow stress and wetting ability than its thermal conductivity.

An existing mathematical model was used to predict the TCC with air as the interface material, and was found to over-estimate the TCC by an order of magnitude. It was found that the model did not accurately predict the effective surface spacing for very smooth surfaces as used in this work. When a modification for smooth contact surfaces

was incorporated into the model it yielded results that were consistent with experimental results.

Thermal Contact Resistances in a Thermal Conductivity Test System

by

Donald A. Schneider

A THESIS

submitted to

Oregon State University

in partial fulfillment of
the requirements for the
degree of

Master of Science

Presented August 18, 1998
Commencement June 1999

Master of Science thesis of Donald A. Schneider presented on August 18, 1998

APPROVED:

Redacted for Privacy

Major Professor, representing Mechanical Engineering

Redacted for Privacy

Chair of Department of Mechanical Engineering

Redacted for Privacy

Dean of Graduate School

I understand that my thesis will become part of the permanent collection of Oregon State University libraries. My signature below authorizes release of my thesis to any reader upon request.

Redacted for Privacy

Donald A. Schneider, Author

TABLE OF CONTENTS

LIST OF FIGURES

LIST OF FIGURES (Continued)

LIST OF TABLES

THERMAL CONTACT RESISTANCES IN A THERMAL CONDUCTIVITY TEST SYSTEM

1 INTRODUCTION

The thermal contact conductance or resistance of an interface is of interest in any application involving the contact of two bodies at different temperatures. If the energy transfer must be estimated, or the temperature drop across the interface known, than at least an approximation of the contact conductance must be available. Current areas of particular interest could include electronics and space applications, to name only two possibilities. The dissipation of the heat generated within an integrated circuit is of crucial importance if the circuit is to perform as designed and for a reasonable time. For this the designer must be able to account for the heat loss and tailor his design accordingly. In space applications the impact of temperature gradients through a structure must be known so that different thermal expansion coefficients can be compensated for to avoid thermal stresses resulting in fatigue and distortion which could render the structure inoperable.

An example of a potential use for thermal conductance data is in the measurement of the thermal conductivity of a solid at a specified temperature. This requires, fundamentally, the measurement of two quantities; the flow of heat energy across a surface, and the temperature gradient perpendicular to the surface and parallel to the heat flow. These two quantities are related to each other, according to Fourier's First law, by a constant of proportionality which is the thermal conductivity, K. Any problem in the theory of heat flow which is soluble can, in principle, be used as a method for measuring K, provided the initial and boundary conditions of theory can be achieved in practice (1).

A common method used for the determination of thermal conductivity is the guarded hot plate method, following the guidelines of the American Society for Testing and Materials (ASTM) standards C-177 and/or C-518 (2, 3). In this method a one

dimensional heat flow is set up along the length of the "stack". The stack consists of a heat source, heat sink, the material under question and some means of measuring the heat flow. The test material is fitted with some means, such as thermocouples, of measuring the temperature gradient along its axis. The entire stack is surrounded by the guard heater, which is maintained at the average stack temperature, to minimize or eliminate radial heat losses. Given the temperature gradient and heat flow, Fourier's First law can be used to calculate the conductivity.

The stack is analogous to an electrical circuit, in which case each element in the stack, and each interface between each pair of elements, represents a resistance. There will be a temperature drop associated with each resistance. The term applied to the resistance at each interface is called the thermal contact resistance (tcr) and is defined as the temperature drop divided by the heat flow. The inverse of the contact resistance is the contact conductance (4).

Sometimes it is difficult or impractical to mount temperature sensing elements directly on a test specimen. In order to minimize the influence of edge effects on the temperature profile, thermocouples are usually mounted at some depth in the sample, often near the centerline. But due to material or geometric considerations, it may impossible to do so. Examples of such situations could include thin specimens, which have insufficient length to establish a meaningful temperature profile, and honeycomb specimens, where only the outer surface temperature is needed. If the surface temperature of such examples could be accurately measured, it would eliminate the need for embedded temperature sensing devices. An added benefit would be reduced sample preparation time and expense. However, the thermal contact resistance makes it difficult to measure the surface temperature with the accuracy needed for material property calculations.

The intent of this work is to investigate and quantify contact resistance and conductance. Specific variables to be explored are the effects of pressure, and the presence or absence to an interface material, and its contribution to the contact conductance. Special attention will be given to the effects of surface roughness, and its effect on the prediction of the contact conductance.

2 LITERATURE REVIEW

Thermal contact resistance depends on several macroscopic parameters: pressure, surface roughness, hardness and interstitial material (5). Heat transfer at the interface occurs by several modes. These include conduction, convection and radiation (6). The contribution from conduction can be further separated into energy transfer through contact of the base material and energy transfer through the interface material. The contribution from convection was generally ignored because for the most part a deformable solid interface material was present. It has also been found to be a very small part of the total energy transfer (6). Likewise the contribution by radiation was ignored due to the relatively low temperatures and small gradients used for testing (5,6). If, however, testing was done at higher temperatures or with a higher temperature drop across the interface the radiation component would need to be accounted for, as radiation is proportional to the fourth power of the absolute temperature, and would increase rapidly.

Numerous articles have been written about efforts to quantify and predict contact conductance. Most approach the subject from the standpoint of surface roughness and deformation under pressure (5,6,7). The actual contact area at the asperities gives a truer picture of contact area than does the nominal area. The contact areas are generally modeled as circular, isothermal spots uniformly distributed over the apparent area (5,6). The actual contact area is then a function of asperity size and slope, material hardness and apparent pressure. In order to correlate the analytical and measured contact conductance it is first necessary to measure and quantify the finish of the opposing surfaces. The surfaces tested in the literature from which empirical data was derived ranged from as-machined, ground, sanded and bead blasted through polished. In general the bead blasted surface results more closely matched the analytical models than did the sanded or ground surfaces (8). This is because of the homogeneous distribution of asperities on the bead blasted surface. The ground and sanded surfaces have a directionally dependent roughness which makes it much more difficult to predict the

actual contact ratio, where the contact ratio is defined as the true contact area of the asperity tips divided by the nominal area.

It has been found that applied pressure affects the contact conductance to varying degrees. For nominally very smooth surfaces, and for hard materials the applied pressure has little effect (7). For rougher surfaces, and if one or both of the surfaces is composed of a material that can deform easily at either the microscopic or macroscopic level, then the pressure can affect the contact conductance. The presence of an interface material can also affect the pressure dependence (4,7,9).

An interstitial material can have a dramatic affect on the contact conductance. The interface material provides a second conduction path, in addition to the asperity contact area. This significantly increases the effective contact area. Materials tested ranged from greases and tapes to metallic foils (4,9). In most cases it appeared that the hardness or flow stress was a larger factor than the conductivity of the material (4,9). Many variables affect the contact conductance. If the interface material is of lower conductivity than the substrate then the penetration of asperities into the interface material will provide the best conduction path and the conductance will increase in comparison to little penetration. If, however the interface material is of similar conductivity to the substrate, then penetration into the interface will have little effect on the conductance.

Many of the mathematical approaches are still largely dependent on empirical constants (6,7,13). An important factor, and one that will be addressed in greater detail later is the effective surface spacing. Two of the mathematical methods proposed to estimate the contact conductance are presented in the following paragraphs.

Rohsenow (7) approaches contact resistance by first defining the interface

conductance as: $$h_i = \frac{q''}{\Delta t_i} \qquad (2.1)$$

where $$q''=-k_1(dt/dx)_1=-k_2(dt/dx)_2 \qquad (2.2)$$

For perfect contact, $h_i \rightarrow \infty$, that is the temperature difference vanishes, or $t_1=t_2$. He states that the three most important effects are interface flatness, joint pressure and mean

interface temperature. His method is then to: 1) calculate the constriction number:

$$C = \sqrt{p / M} \qquad (2.3)$$

where p is the contact pressure and M is the Meyer hardness of the softer contact material; 2) estimate the effective gap thickness as:

$$l=3.56(l_1+l_2) \text{ if } (l_1+l_2) < 280 \ \mu\text{in.} \qquad (2.4a)$$

for smooth contacts or:

$$l=0.46(l_1+l_2) \text{ if } (l_1+l_2) > 280 \ \mu\text{in.} \qquad (2.4b)$$

for rough contacts, where l_1 and l_2 are the RMS depths of surface roughness; 3) calculate the gap number: $B = 0.335C^{0.315\sqrt{A}/l^{0.137}}$ (2.5)

where A is the surface area: 4) estimate the equivalent conductivity of interstitial fluid as: $k_f = k_0$ (2.6)

for liquids, evaluated at the mean interface temperature, or:

$$k_f = \frac{k_o}{1+\dfrac{8\gamma(\frac{\nu}{\upsilon})(a_1+a_2-a_1a_2)}{\mathrm{Pr}(\gamma+1)a_1a_2 l}} + \frac{4\sigma l \varepsilon_1 \varepsilon_2 \bar{t}_i^{\,2}}{\varepsilon_1+\varepsilon_2-\varepsilon_1\varepsilon_2} \qquad (2.7)$$

for gases, where k_0 is gas conductivity at zero contact pressure; Pr is the Prandtl number, $\bar{\nu}$ is the mean molecular velocity, γ is the ratio of specific heats, and υ is the kinematic viscosity of the gas evaluated at $\bar{t}_i$; a and ε are the accommodation coefficient and emissivity of the contact surfaces evaluated at t_1 or t_2; and σ is the Stefan-Boltzmann radiation constant; 5) calculate conductivity number:

$$K = k_f(k_1+k_2)/2(k_1k_2) \qquad (2.8)$$

where k_1 and k_2 are conductivities of the two solids evaluated at:

$$\frac{t_1+(k_1t_1+k_2t_2)/(k_1+k_2)}{2} \qquad (2.9a)$$

or

$$\frac{t_2+(k_1t_1+k_2t_2)/(k_1+k_2)}{2} \qquad (2.9b)$$

6) using B/K and C, enter **Figure 2.1** and determine interface contact conductance h_i. This method does not take into account solid interface materials.

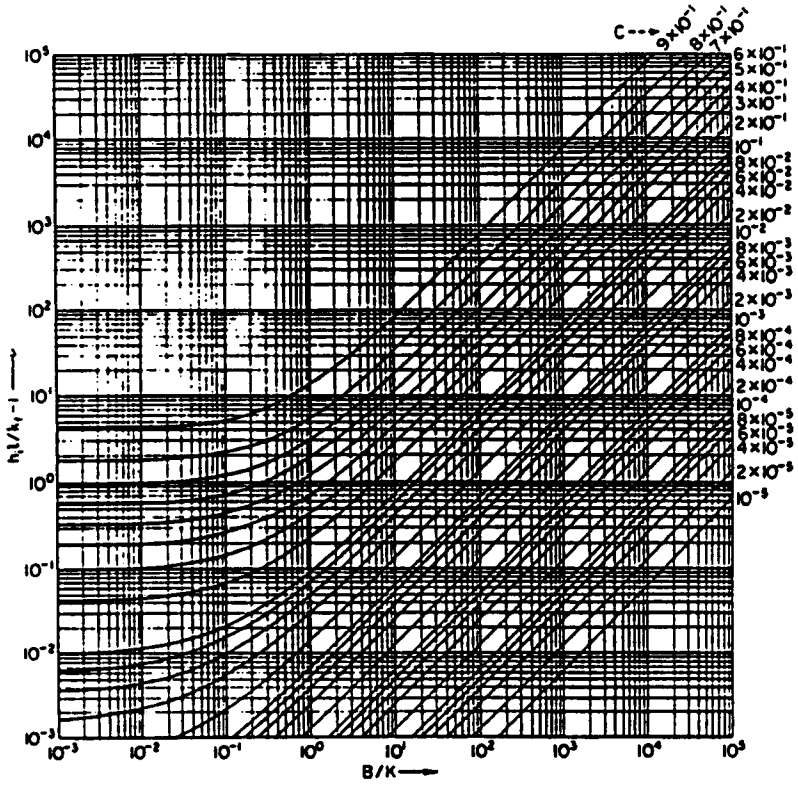

Figure 2.1 Thermal interface conductance theory (7).

Hsieh and Touloukian (6) attempt to correlate the literature data of thermal conductance in terms of derived dimensionless groups. Surfaces covered include nominally flat and nominally wavy surfaces. They also considered two cases, when the contact radius is treated as constant, and when the radius is variable as a function to the roughness. The assumption is made that the asperities are right circular cones of equal apex angles with their bases resting on a common plane, with the distribution of asperities both isotropic and homogeneous. Both plastic and elastic deformation are taken into account. Solid-solid conduction was derived by Holm as:

$$h_s = 2n\bar{a}\lambda_s \qquad (2.10)$$

where h_S is the solid-solid conductance, n is the number of asperities which are engaged in contact, $\bar{a}$ is the mean contact radius of asperities and λ_s is the thermal conductivity of the materials involved. Solid-fluid-solid conductance can be expressed as:

$$h_g = \lambda_g / \delta_{eg} \qquad (2.11)$$

where h_g is the fluid conductance, λ_g is the thermal conductivity of the interfacial fluid and δ_{eg} is the equivalent gap thickness. In deriving Holm's equation the radius of the model cylinder is defined as:

$$n\pi\bar{r}_e^{\,2} = 1 \qquad (2.12)$$

where $\bar{r}_e$ is the mean radius of the cylinder. If only plastic deformation of the tips of the asperities is considered, the radius of the actual contacts is:

$$\bar{a} = r_e(p / 3Y)^{1/3} \qquad (2.13)$$

where p is the apparent loading pressure and Y is the yield stress of the material involved. By using these four equations, the following dimensionless equation is derived:

$$\frac{h_t\delta_{eg} / \lambda_g - 1}{\lambda_s\delta_{eg} / \bar{a}\lambda_g} = \lambda(\frac{P}{Y}) \qquad (2.14)$$

where $\lambda = 2 / 3\pi$ and h_t is the total contact conductance. Examination of this equation shows that the variables are combined into dimensionless groups. The numerator on the left is the total contact conductance divided by the fluid conductance. The denominator on the left is the ratio of thermal conductivities divided by the ratio of the radius of the contact spot to the equivalent gap thickness. P/Y is the ratio of loading pressure to the material yield strength. The numeral one in the numerator represents the contribution due to fluid conductance, which for contacts in a vacuum reduces to zero.

A variety of literature data for nominally flat surfaces with the asperity radius assumed a constant 30 μm was plotted on a log-log graph. With the left side of equation 14 being the ordinate, p/Y the abscissa and λ the slope of an imaginary line, the data agreed well with the line representing the theoretical value at low and medium pressures, but data for surface roughness of less than 10 μin. curved above the line at higher pressures. The deviation of the correlated results from the theory is an indication that the constant radius of contact spots assumption is not a realistic one.

A model was proposed which took into account the variable radius of asperities as a function to surface roughness. The radius of contact spots was derived and given as:

$$\bar{a} = \sigma\tan\gamma(\frac{P}{3Y})^{1/2} \qquad (2.15)$$

where γ is the apex angle of the model asperities, $\sigma = (\sigma_1^2 + \sigma_2^2)^{1/2}$ and σ_1 and σ_2 are the average roughness' of the two contacting surfaces. When the preceding literature data was re-plotted using this modified expression, it showed a good convergence with the theoretical line of slope 1.07. Again, this model did not take into account a solid interface material.

3 EXPERIMENTAL APPARATUS

The objective of the experimental apparatus was to use a heat source and a heat sink to establish and maintain a steady state heat flow along the longitudinal axis of the test specimen. The temperature gradient and heat flux along this axis would have to be measured accurately and precisely. The radial heat losses would have to be minimized so that what was being measured was the heat flow between the source and sink and not the loss or gain to the environment. The test device would also require some means to measure the compression force exerted in the longitudinal direction of the test piece.

All experimental procedures were performed on a system shown schematically in **figure 3.1**. The setup included a guarded hot plate fixture, personal computer with data acquisition card, solid state relays (SSR), solenoid valve, liquid nitrogen tank, load cell with digital display and an AC variac. The test specimens were of stainless steel.

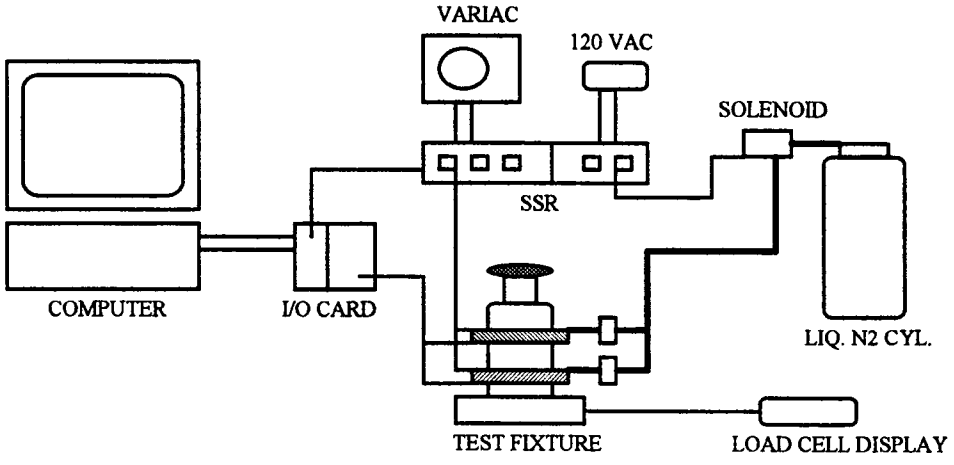

Figure 3.1 Test apparatus.

The guarded hot plate fixture was constructed of copper upper and lower plates, stainless steel guide rods and plates, and aluminum support pieces, as shown in **figure**

3.2. The various materials were chosen for their high conductivity (copper), low conductivity (stainless steel) and ease of machining (aluminum). The large knurled knob at the top of the fixture controlled the clamping load, while the load cell at the bottom monitored the load. The holes in the plates which rode on the guide rods were drilled slightly over-sized to allow the plates to conform to slightly out of parallel specimen surfaces. A ball bearing under the bottom plate, and the rounded tip on the clamping rod above the upper plate helped to facilitate this compliance. Centrally located thermocouples provided the signal for temperature monitoring by the analog input part of the data acquisition system. Digital output from the data acquisition card operated the solid state relays which cycled on and off to control current to the resistance heating and liquid nitrogen solenoid.

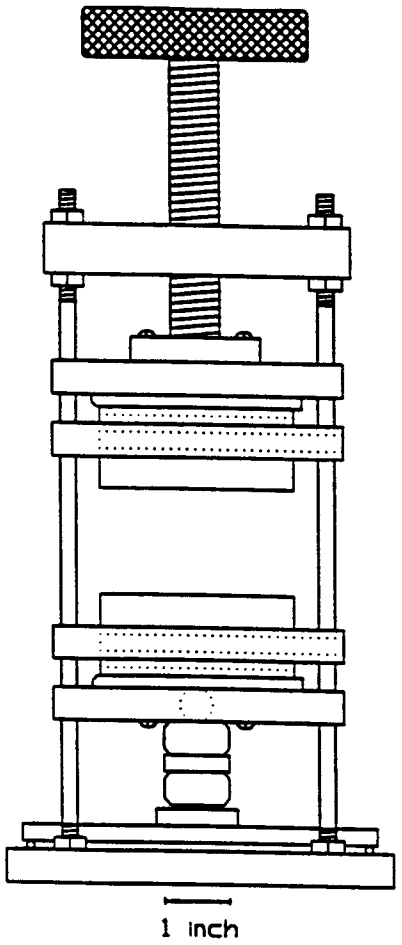

Figure 3.2 Test fixture.

The heart of the system is the copper upper and lower plates, shown in **figure 3.3**, which provide the temperature differential to drive the energy transfer. Copper was chosen for this portion of the fixture due to its high conductivity and resulting small temperature gradient in the traverse direction. The contact surfaces measure two inches by three inches. The plates contain passageways for liquid nitrogen cooling and grooves for resistance heating. The coolant passages were drilled into the solid copper in a double-j pattern, with the unnecessary holes and passages tapped and plugged. The inlet and exhaust ports were fitted with barb type fittings for connection with rubber hoses. The heating grooves were machined into the surface of the plates opposite the contact surface. Ni-chrome wires contained in ceramic ferrules were put in the grooves and held in position with stainless steel plates. Stainless steel was chosen for this duty due to its relatively low thermal conductivity and high heat tolerance.

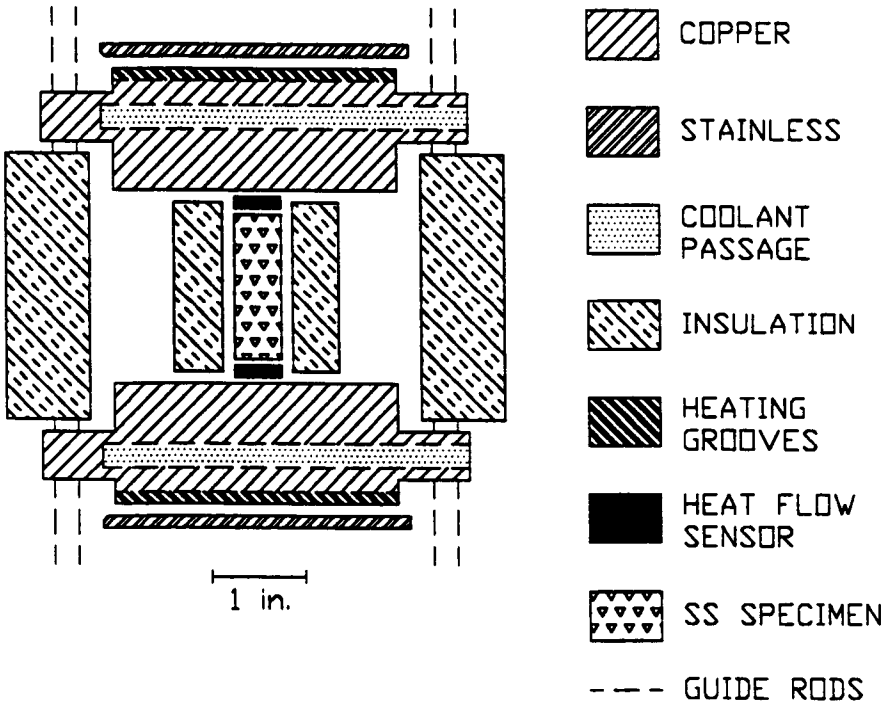

Figure 3.3 Guarded hot plate with insulation.

Radial heat losses were minimized by a passive guard heater also shown in **figure 3.3**. Going from the inside toward the outer surface, the insulation consisted of the following: one layer of Kaowool (quartz cloth) around the specimen; four layers of aluminum foil; one layer of copper foil; one or two layers of corrugated cardboard; 0.25 inch plywood; and approximately one inch of Styrofoam. The entire package was held in place by a rubber band. The Kaowool was used to suppress convection currents from directly contacting the specimen and was chosen for its low thermal conductivity and high temperature tolerance. The aluminum foil was chosen for its radiative insulating ability and to function as a vapor barrier. The purpose of the copper foil, in conjunction with the aluminum foil was to act as a limited conduction path between the upper and lower plates, with the intention of creating a linear temperature gradient parallel to the test specimen. The Styrofoam was chosen for its extremely low thermal conductivity. Over time it was found that the Styrofoam would melt and recede from contact with the hotter surfaces, resulting in loss of insulation. The cardboard was placed in front of the Styrofoam to act as a thermal barrier, with limited success. It was visually apparent that the foam would still require replacement after several tests, but no loss of insulation was observed, as indicated by no measured difference between the upper and lower heat flow sensor readings during successive tests. The intent of the insulation package was to minimize radial heat losses while having a small heat capacity, and thus to limit the time for the stack to reach steady-state conditions. Successful operation of the passive guard heater avoided the need for an active guard heater. It was felt that improper use of an active guard heater could induce errors and inconsistencies in the data.

Electronic monitoring, control and data acquisition was provided by an Analog Connection™ ACPC-16 16 bit system from Strawberry Tree Inc. running from a personal computer. This card had 8 analog input channels for monitoring of temperature and heat flux, and up to 16 digital input/output channels for control of resistance heating and nitrogen cooling. The system software allowed for either fixed set point or time list controlled temperatures. Most of the tests were done at the temperatures listed in **table 4.1**, with a 30°C temperature difference between the hot and cold plates.

The solid state relays (Electrol, Inc., #7808) were chosen for their ability to cycle on and off rapidly. They provided the switching to power the heating elements and the coolant flow solenoid. The signal that operated the solid state relays came from the five volt digital source on the data acquisition card. For the resistance heating, power came from an AC variac, which was typically adjusted between 20 and 45 volts. The nitrogen flow was controlled by a J.C. Controls SLV-40, 120 VAC solenoid valve. The load on the stack was continuously monitored with an Omega Engineering Inc. load cell and digital display, model numbers LCG-500 and DP-350, respectively.

The stainless steel test pieces had a cross section of 0.500 inch by 0.625 inch and were 1.50 inches long. The first piece was solid and was used to establish a baseline temperature profile. The second was identical in length, but was split at the midpoint of the length, making a symmetrical pair. The split pair was used throughout the experiment to test different interface materials. Both pieces were drilled and fitted with thermocouples as shown in **figure 3.4**. The thermocouple spacing was identical on both. The pieces were machined and drilled on a Bridgeport milling machine, using the digital table travel display to precisely locate the thermocouple holes. The contact surfaces were finished on 600 grit wet/dry sandpaper, with a unidirectional sanding motion. This produced a surface roughness of 0.0708 micron (RMS) parallel to the sanding marks and 0.0482 micron (RMS) perpendicular to the sanding marks as measured with a Tencor Instruments Alpha-Step 100. All the test pieces were machined from the same bar stock and in the same direction, to eliminate any inconsistency due to material anisotropy.

Heat flux measurement was provided by a pair of Concept Engineering model FS-60 sensors, with one each placed at the top and bottom of the test specimen. The selected sensors had the same cross sectional area as the test specimens. The sensors were calibrated as a pair as described in a later section.

In an effort to isolate the load cell from thermally induced strains, leading to erroneous pressure readings, the column under the lower plate, as shown in **figure 3.2** was constructed. The column consisted of a 1.0 inch diameter by 0.25 inch thick disc of Zerodur material sandwiched between cylindrical aluminum rods. The Zerodur disc was chosen for its low thermal conductivity. The bottom piece of aluminum had a recess

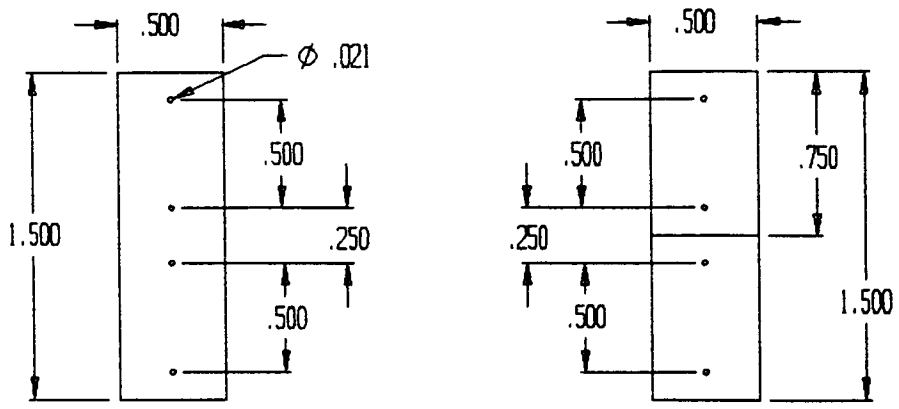

Figure 3.4 Solid and split test specimens.

machined into the lower surface to fit the stud on the top of the load cell. This prevented tipping and aided alignment during assembly. The top aluminum piece had a tapered hole drilled into its top surface to locate and secure the 0.50 inch ball bearing. The aluminum cylinders were chamfered on either end to reduce the conduction path, and the limited contact area of the ball bearing also impeded heat transfer.

Early in testing it became apparent that the load on the stack could change rapidly and significantly. As the fixture was relatively rigid, was constructed of materials with widely varying thermal expansion coefficients, and possibly heated non-uniformly, temperature changes could lead to undesirable pressure fluctuations on the test specimen. In an effort to moderate these abrupt load changes, and to make load control easier, a spring was added under the load cell. This spring consisted of a piece of aluminum bar stock, 1.0 inch wide by 0.25 inch thick, laid flat. It was simply supported on either end by 0.125 inch steel rods. In the absence of this spring the load could change by nearly a factor of 2 over the test temperature range if not adjusted. With the spring in place the load would change by about 10 % without adjustment, and could be maintained to within about 1-2 lb. with monitoring and adjustment.

4 EXPERIMENTAL PROCEDURES

The test procedures were designed to establish guidelines to follow for the course of the project. In this way the experiments could be performed in a consistent manner and any trends between subsequent tests would become evident. The objective was to maintain a consistent temperature difference across the length of the test apparatus. A temperature difference (delta T) of 30°C across the fixture was selected because in previous conductivity tests this was found to produce a meaningful gradient and heat flux in test specimens of similar conductivity.

In addition, a limited number of tests were performed with a delta T across the stack of 20 °C and 40 °C. The intention was to determine if the conductance was constant for a given set of parameters, including pressure and interface material, and independent of the temperature gradient, and thus the heat flow, through the stack.

All tests were performed at standard temperature and pressure in air. With all instrumentation connected to the data acquisition system, the test piece was placed in the fixture and all insulation installed. The load was adjusted to the desired pressure, and thereafter continuously monitored and adjusted to compensate for temperature effects. The testing then progressed through the temperature steps as detailed in **Table 4.1**.

Table 4.1 Test temperature profile.

Time (min.)	Average Temp. (°C)	Hot Plate Temp. (°C)	Cold Plate Temp. (°C)
0-35	0	15	-15
35-1:05	20	35	5
1:05-1:35	40	55	25
1:35-2:05	60	75	45
2:05-2:35	80	95	65
2:35-3:05	100	115	85

The data acquisition software was set up to record the measured variables at thirty second intervals. These variables included the sample temperature profile, the temperatures of the upper and lower plates and the heat flow. This was done by writing to a separate data file. At the conclusion of each test the data file was copied to a separate diskette for further analysis. For each successive test the interface material was changed and/or the pressure was changed. In some cases the test was repeated at a previously used pressure with the same interface material or a new piece of the same material. The purpose of these repeat tests was to look for the effects of permanent deformation and/or work hardening. **Table 4.2** lists the details of various interface materials and pressures tested. At the conclusion of each test, the interface material was removed and inspected, if changed, and the details recorded.

The data files were then imported into a commercial spreadsheet (Quattro Pro) for analysis. Typically the final ten data points at each temperature step were averaged for calculation of the desired information. Given the temperature gradient between the thermocouples and the distance to the interface, the temperature at each side of the interface was found by extrapolation. The difference between adjacent surface temperatures was then the drop across the interface. The contact resistance was found by dividing this number by the heat flux as measured by the heat flow sensors. The contact conductance is merely the reciprocal of the contact resistance.

Table 4.2 Test details.

Interface Material	Test Load (lbs.)	Comments
none	N/A	solid test piece
none	50	
	200	
Indium foil	25	new piece
	50	re-used from previous test
	100	re-used from previous test
	250	re-used from previous test
	50	re-used from previous test
	250	new piece
	250	re-used from previous test
Teflon tape Mil-Spec. T-27730A	25	new piece
	50	new piece
	100	new piece
	250	new piece
Heat Sink Compound (silicone grease)	25	new material
	50	new material
	250	new material
Colloidal Silver Paint	25	new material
	50	new material
	100	new material
	250	new material
Copper Foil (annealed)	25	new piece
	50	re-used from previous test
	100	re-used from previous test
	250	re-used from previous test
	250	new piece
Different delta T		
Heat Sink Compound	50	new material (delta T = 20 °C)
	50	re-used from previous test (delta T = 40 °C)
Teflon tape	100	new material (delta T = 20 °C)
	100	re-used from previous test (delta T = 40 °C)

5 CALIBRATION

Heat flow information during testing was provided by a pair of thermopile based heat flow sensors. One each was placed at the top and bottom of the stack, nearest to the hot and cold plates. The output from the sensors was voltage, and the manufacturer supplied a calibration number to convert this to W/m^2. Prior to using the information from the heat flow sensors it was necessary to calibrate them with a known standard. A stainless steel standard reference material (SRM) supplied by the National Institute of Standards and Testing (NIST) was used to calculate the true heat flow through the stack. The SRM was supplied with a table of conductivities at certain temperatures.

The SRM, with a known cross sectional area, had 0.024 inch diameter holes drilled from the side at a carefully measured distance apart, in which 0.003 inch diameter wire T-type thermocouples were inserted. Because the conductivity of the SRM as a function of temperature was known, the temperature gradient between the thermocouples could then be used to calculate the true heat flow. For this calculation, Fouriers equation for one-dimensional heat flow was used:

$$Q_{act} = -k_{SRM}\frac{dT}{dx} \qquad (5.1)$$

where: Q_{act} is the heat flow, k_{SRM} is the thermal conductivity of the stainless steel reference material, dT is the temperature difference between the thermocouples and dx is the axial thermocouple spacing.

It was found that the heat flow, as calculated from the temperature gradient in the SRM was approximately 50% higher than the value indicated by the heat flow sensors, and was also dependent on the average temperature at which the measurement was taken. **Figure 5.1** shows the raw data obtained from a typical calibration test. The lower line is the average of the heat flux sensor outputs, while the upper line is the computed heat flux based on the temperature gradient in the NIST SRM. The periodic dip in each curve corresponds to the transition from one temperature step to the next, as listed previously in **Table 4.1**. This is caused by the lag in temperature rise in the test specimen due to its heat capacity. As the test fixture ramped up to the next higher temperature step, the upper

heat flow sensor recorded a higher flux. But because the lower plate was temporarily hotter than the test specimen there was a reversal of heat flow through the lower flux sensor. The average of the outputs from the two heat flow sensors then showed a lower value until the test specimen approached the desired average temperature. The reason for the extra dip in each curve between the 100th and 150th time step is not certain, but may have something to do with an imbalance in the liquid nitrogen flow.

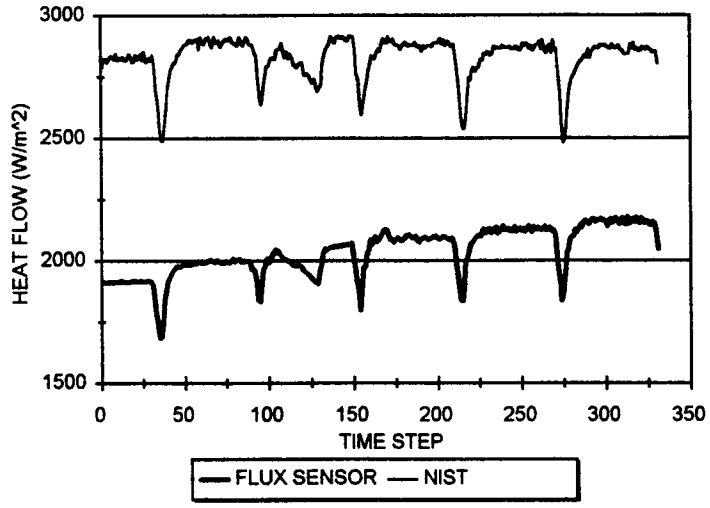

Figure 5.1 Sensor calibration data for 30 °C temperature drop across fixture.

Inspection of **figure 5.1** would seem to indicate that the true steady state heat flow is relatively constant with time (and temperature), while the average output of the heat flux sensors (Q_{ave}) is approximately a linear function of temperature. A straight line superimposed over either curve would coincide with the steady state portion of the data. Due to the apparent linearity of both curves it was theorized that the expression for the actual heat flow would be of the form:

$$Q_{act}=Q_{ave}(mx+b) \qquad (5.2)$$

where m is the temperature correction, x is the average test temperature and b is a constant. This equation was then rearranged:

$$Q_{act}/Q_{ave} = mx + b \qquad (5.3)$$

where the term on the left was the dependent variable and x was the independent variable. A linear regression was then performed on the data shown in **figure 5.1** using the advanced math menu in Quattro Pro to solve for the slope and intercept. The temperature correction, m, and intercept, b, for temperature drops across the fixture of 20 °C, 30 °C and 40 °C are shown in **table 5.1**. Given these constants the true heat flow could be estimated by reorganizing the equation again in the form:

$$Q_{est} = Q_{ave}(m * T + b) \qquad (5.4)$$

Table 5.1 Calibration correction constants.

Fixture Delta T	Temperature Coefficient	Intercept
20 °C	-0.00141	1.420853
30 °C	-0.00157	1.470042
40 °C	-0.00152	1.418001

The results of this calibration are shown in **figure 5.2** for a 30 °C fixture temperature drop over a range of 0°C to 100°C. In this figure the estimated true heat flow is very nearly exactly superimposed over the SRM predicted curve. It is apparent from this curve fit that the assumption of a linear correction factor is adequate over this temperature range. The corrected heat flux for 20 °C and 40 °C fixture temperature spans have similar appearances but with a higher or lower output, depending on the delta T.

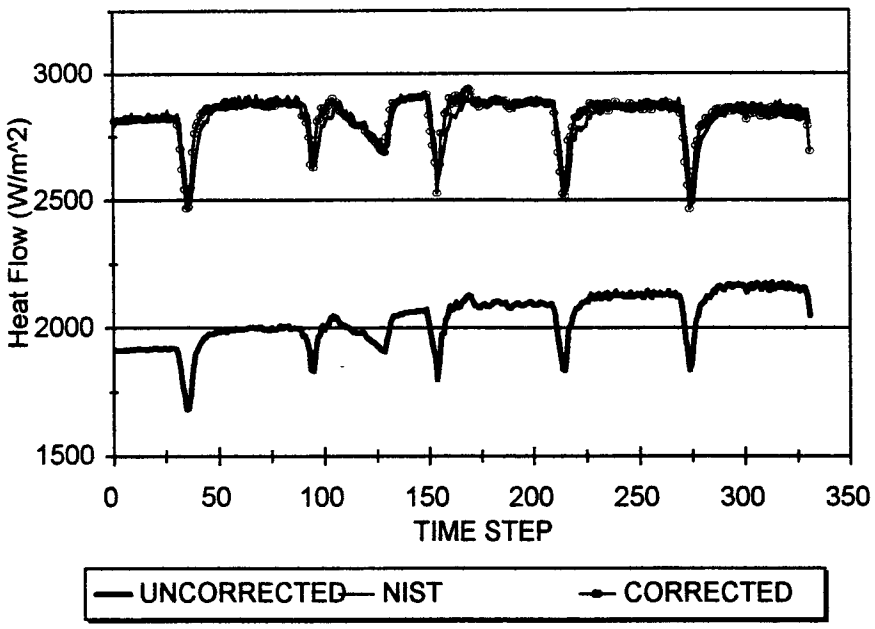

Figure 5.2 Calibrated heat flux for 30 °C fixture span.

In order to facilitate the use of a spread sheet to calculate the true heat flux, it was helpful to formulate an equation for the conductivity of the SRM as a function of temperature. A linear regression was used to fit a straight line to the conductivity values supplied by the NIST. Three data points that covered the temperature range of interest were used. Although the conductivity is not strictly a linear function of temperature, the error in assuming so over a limited temperature range was less than 0.2 %. The resulting equation:

$$k = 0.018914 * T + 13.77358 \qquad (5.5)$$

where T is temperature (°C), was then input into cells in the spreadsheet used to calculate the actual heat flux. By so doing, the conductivity of the SRM could be accurately approximated for any temperature within the test range. The R-Squared value for the regression was 0.999446.

Throughout the testing it was assumed that the heat flow was unidirectional, that is that all energy transport was along the stack, and that radial loses were minimized or eliminated. In fact later testing would indicate that radial heat losses were effectively minimized, and that any remaining losses were accounted for by the calibration method.

According to ASTM standard C-518 (3), the heat flow sensor must be calibrated every 30 days in order to be considered accurate. All of the testing for this thesis was done within a reasonable time period after calibration. Subsequent calibration tests at a later date showed that the calibration factors were within a few percent of the initial values.

6 EXPERIMENTAL RESULTS

As shown previously in **Table 4.2**, the tests were done with various interface materials and at varying loads. A typical series of tests would begin with fresh interface material, if used, at the lowest load, with each successive test at a higher load. In some cases the interface material was changed after each test, while other test series used the same piece of material for the entire series. In order to test for the effects of strain hardening, permanent deformation and chemical changes, other test strategies were also used. These included re-testing at a reduced load, using a new piece of interface material to repeat a test, and identically repeating the previous test, either with or without new interface material. With these variations in test methods, it was hoped that any equipment failure or error in test procedures would become evident.

Solid Test Specimen

The first test was performed on the solid stainless steel sample to verify correct thermocouple and guard heater operation, and to determine the time necessary to reach steady state conditions. This was then the baseline for all subsequent tests. It was felt that if the guard heater was performing as planned the result would be a linear temperature profile along the sample, which would verify that radial heat losses had been minimized. **Figure 6.1** shows the temperature profile of the solid specimen, at an average temperature of 100 °C. An important feature of this graph is that the temperature profile is virtually a straight line, which is consistent with Fourier's law, a first order equation. What this also illustrates is the effectiveness of the passive guard heater arrangement. The linear temperature profile for the solid test piece is an indication that the heat flux is constant along the length of the piece. If the radial heat losses were significant, or the sample had not yet reached steady state, this would result in a curved temperature profile.

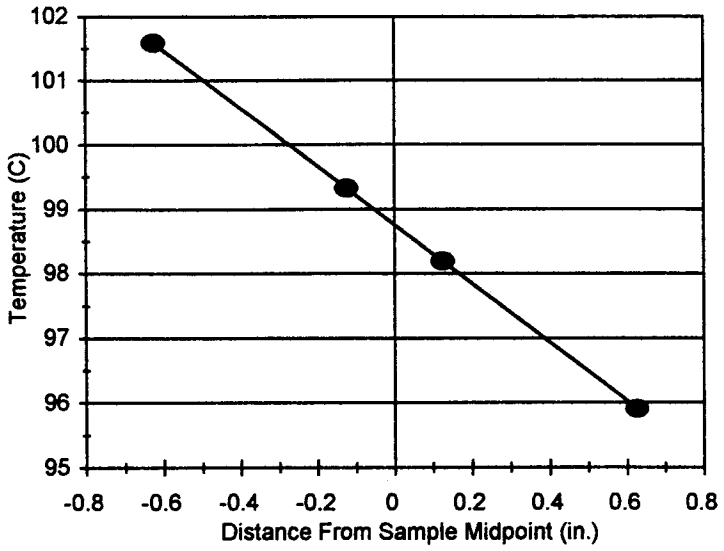

Figure 6.1 Temperature profile of solid test piece

Split Test Specimen With No interface Material

The next series of tests were done on the split sample with 50 lb. and 200 lb. loads, but with no interface material. The sample temperature profiles for both tests are shown in **figure 6.2**. The vertical distance between points on the centerline represents the estimated temperature drop across the interface, calculated by extrapolating from the nearest thermocouple location to the interface. While the average temperature differs somewhat between the two loads, the gradients are similar and interface temperature drops differ by less than 8 %. As would be expected, the test with the higher load had the smaller temperature drop across the interface. Another important feature of this graph is the comparison between profiles for the solid piece, in **figure 6.1**, and split test piece, in **figure 6.2**. While the two profiles for the split test piece are nearly parallel, they have a shallower slope than the solid test piece. This is caused by the added resistance of the interface, which is not present in the solid piece, resulting in a slight decrease in heat flow and gradient. The slope of the temperature profile is also constant on either side of the interface for each of the tests. The slope of this line is dT/dx in equation 5.1.

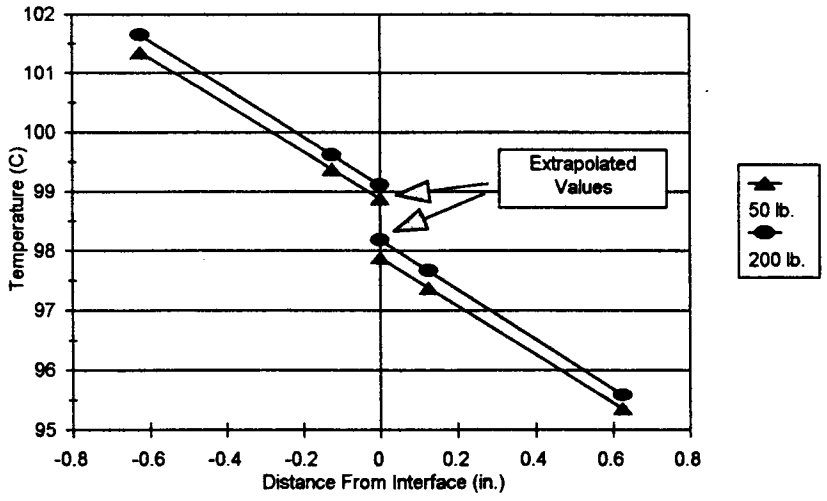

Figure 6.2 Temperature profile of split test piece with no interface material.

Figure 6.3 shows the temperature drop over the whole test range for the split sample. The interface temperature drop remains constant at ≈ 1 °C. There appears to be little if any pressure or temperature dependence at these load levels. These pressures are probably too low to cause the deformation that would result in increased contact area for a material as hard as stainless steel.

Indium Foil

The next series of tests used 0.0015" indium foil at the interface. Indium is a soft material with a conductivity of ≈24 W/m/K. The initial series was done at loads of 25, 50, 100, 250 and again at 50 lbs. As **figure 6.4** shows, the tests through 250 lbs. show a slight decrease in temperature drop (increase in conductance) with increasing pressure. The test was then repeated at 50 lbs. with the original piece of interface material. The results are the same as the original data points, within the limits of precision of the thermocouples.

A new piece of indium foil was installed and the test repeated with a 250 lb. load. It was then repeated again with the same load and interface material, with some

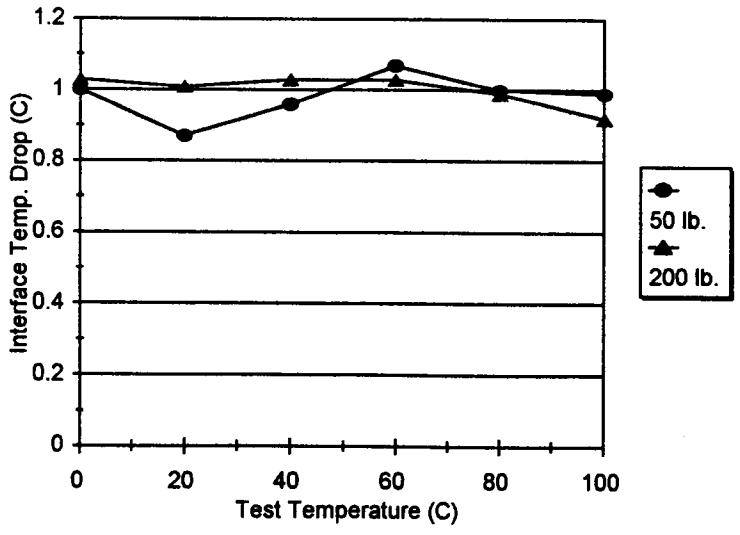

Figure 6.3 Interface temperature drop with no interface material.

interesting results. **Figure 6.5** shows these results, along with the original 25 lb. and 250 lb. data points for reference purposes. At the lower temperatures the first repeat test showed data points that are similar to the original 25 lb. load points. But at higher

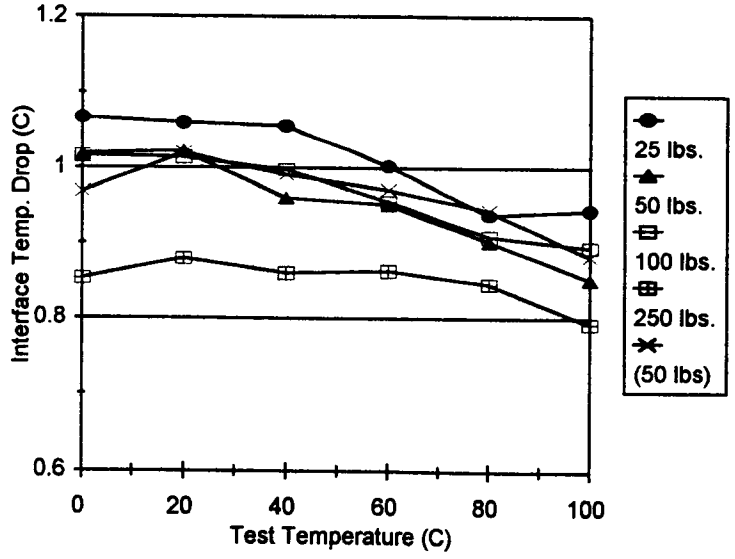

Figure 6.4 Interface temperature drop with indium foil at interface.

temperatures the data points approach the original 250 lb. data points. The second repeat at this load had data points intermediate to the original 25 and 250 lb. data points. What is interesting is that the terminal point, at 100 °C, is identical for all three tests with a 250 lb. load. This suggests that there is not only a pressure dependence, but that the conductance might also be a function of deformation due to time, temperature and maybe even the number of loading and temperature cycles. In all of these tests, the interface temperature drop was approximately the same as with no interface material at all (≈1 ° C). If there was any improvement in conductance due to presence of the indium foil, it

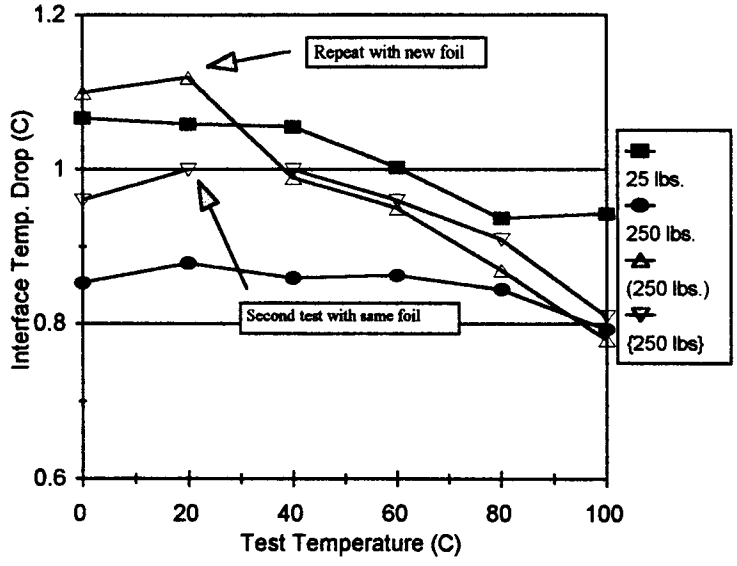

Figure 6.5 Indium foil test repeated with new interface material.

was approximately offset by the increased resistance of the bulk indium plus the addition of a second interface. Also, the conductivity of indium is not that much higher than stainless steel. Inspection and measurement of the indium foil after testing showed no permanent thinning within the resolution of the measuring device (0.0005").

Teflon Tape

The next series of tests used 0.001" Teflon tape, Mil-Spec T-27730A, as the interface material. Teflon tape might be the material of choice in applications that allow no contamination of the test material. The resulting temperature drops are shown in **Figure 6.6**. The difference decreased through the 25, 50 and 100 lb. tests, but leveled off between the 100 lb. test and the 250 lb. test. Inspection of the Teflon tape after each test showed substantial and uneven thinning. It appears that at the 100 lb. load the flow stress of the material has been exceeded, giving no benefit to increased loading. The conductance may also be aided by Teflon's lubricating ability (4). The uneven thinning may be evidence of non-flat (wavy) contact surfaces, or non-parallel contact. At 100 and 250 lb. loads the temperature drop (≈0.5 °C) is less then that for no interface material and

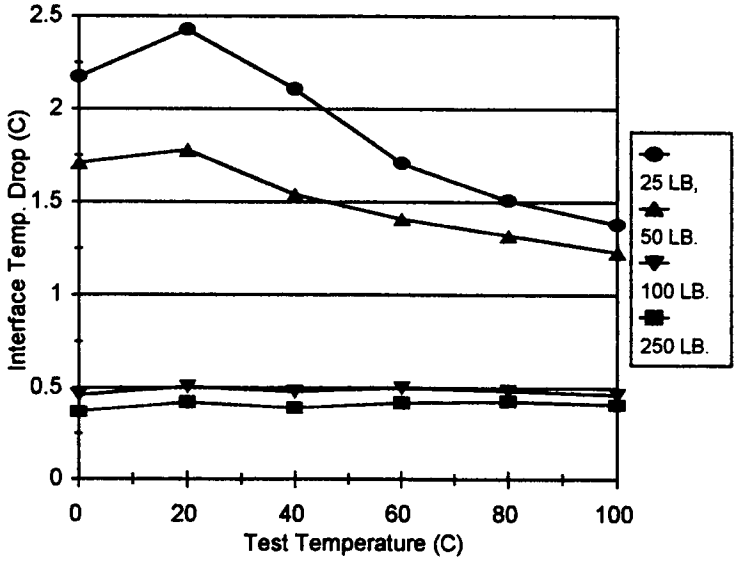

Figure 6.6 Temperature drop with Teflon tape at interface.

indium foil (≈ 1.0 °C). There is no readily apparent reason for the "hump" in the data at the lower pressures.

Heat Sink Compound

The material for this series of tests was a silicone grease based heat sink compound (70% polysiloxane, 30% zinc oxide), with a conductivity of ≈0.4 W/m/K, available from Radio Shack. These tests were done at 25, 50 and 250 lb. loads. The material was cleaned and replaced after each test. As **Figure 6.7** shows, there is no significant change in temperature drop over this pressure range. What difference is evident is approximately the same order of magnitude as the electrical noise in the thermocouple signal. The temperature drop is ≈0.2 °C over the entire temperature range, which is the lowest value yet. Even at 25 lb. the flow stress of the material has been exceeded. While the silicone grease has fairly low conductivity, it also improved the

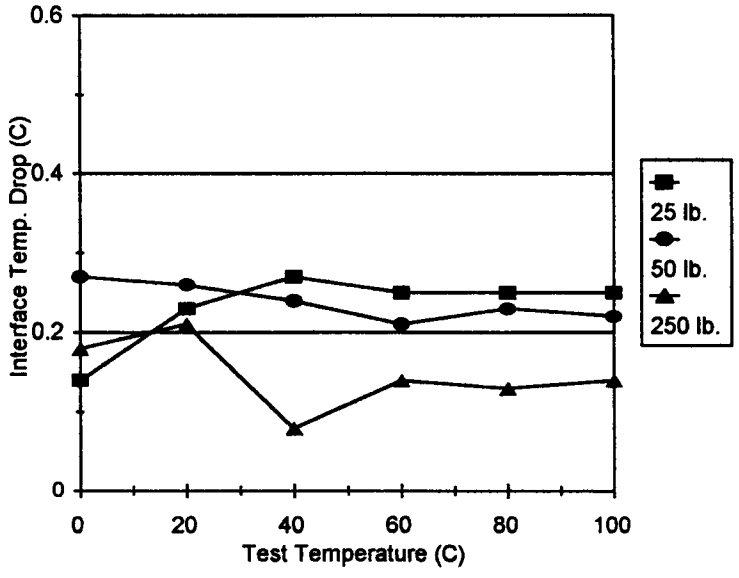

Figure 6.7 Temperature drop with heat sink compound at interface.

conductance the most. As theorized earlier, it is probably the low flow stress more than the conductivity of the interface material that improves the conductance (4,9). Additionally, the wetting ability of the grease probably improves the contact conductance. At the conclusion of each test, the grease was cleaned from the contact

surfaces and replaced. At this time it was observed that the grease was thicker and more viscous than at the beginning of the test. Apparently the testing had changed the grease properties, perhaps by out-gassing some of the more volatile materials.

Silver Paint

This material was a colloidal silver paint, supplied by Energy Beam Science, Inc., P-CS-30. It was applied with a small brush immediately prior to assembly and application of the load. It dried rapidly and tended to bond the contact surfaces, requiring significant force to separate the two halves after testing. The interface material was removed after each test, using the solvent/extender supplied with the paint. As **Figure 6.8** shows, there is no apparent pressure effect on the conductance or temperature drop. The drop was ≈0.2-0.3 °C over the temperature range, and there is no apparent trend due to

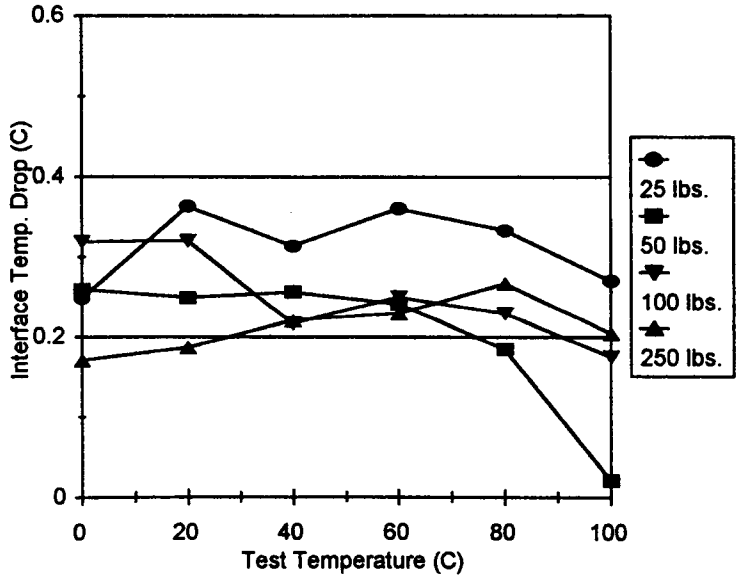

Figure 6.8 Temperature drop with silver paint at interface.

pressure. Again the variation over the test spectrum is not much more than the noise in the thermocouples. It is likely that the silver paint bonds the surfaces in a manner that is similar to soldering.

Annealed Copper Foil

The starting material for this interface was 0.0015" copper foil. The foil was first cleaned with a 600 grit wet/dry sandpaper to remove oxidation and surface contamination. It was then treated with a silver brazing flux prior to heating to remove and prevent further oxidation. A propane torch was used to heat the foil, followed by a water quench. It was again cleaned, with a flux containing zinc chloride and hydrochloric acid, followed by a water rinse. No hardness testing was done prior to use, due to the extremely thin section, but in handling the annealed foil, it was apparent that is was significantly softer than as it came from the roll.

Testing was done at loads of 25, 50, 100, 250 lbs., with the same piece of foil, and again with a new foil at 250 lbs. As shown in **figure 6.9**, this test series showed a distinct trend towards lower contact resistance with increasing pressure. At the 0 °C data point, the 25 lb. test had a temperature drop of ≈1.7 °C, while the 50, 100 and 250 lb. tests had drops of 1.65, 1.47 and 1.3 °C, respectively. All of the curves are of similar shape, with a distinct trend towards lower resistance with increasing temperature.

Figure 6.9 also shows the results of a second test with new foil at a 250 lb. load. The curve has a shape very similar to the previous tests, with the same decreasing resistance with increasing temperature. The temperature drop is, however, less at each data point than for the previous 250 lb. test. As this test used all the same hardware (thermocouples, insulation, etc.) and procedures as previous tests, it is possible that the difference in results is attributable to a difference in interface material properties. Possibly the new copper foil was somewhat softer due to a slight difference in annealing procedures, and therefore deformed somewhat easier. It is also possible that the previous interface piece experienced some degree of work hardening due to the loading and

unloading cycles, and cycling through the temperature range. This would have made it somewhat more resistant to deformation at each successively higher load, resulting in less conformance or deformation, and therefore making less improvement in conductance.

Heat Sink Compound With Delta-T of 20°C and 40°C

This series of tests differed from the first series in that the temperature differential across the fixture was the variable, while the load was held constant at 50 lbs. The temperature range and step size was the same as before, from 0 °C to 100 °C, in 20 ° C increments. For the first test a 20 °C differential was maintained across the fixture, while for the second test the differential was increased to 40 °C. The intention of this test variation was to determine if the contact conductance was constant, that is, independent of the temperature differential and resulting heat flux. In order to minimize any

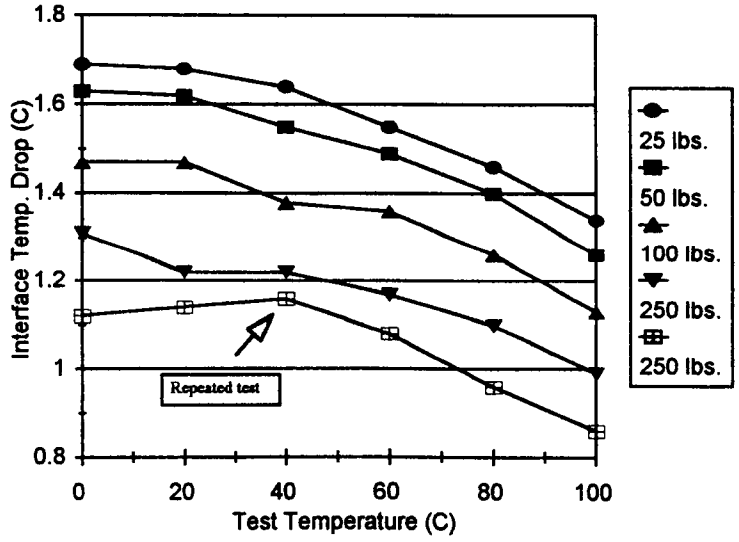

Figure 6.9 Temperature drop with copper foil at interface.

disturbance to the test set up, which might result in some variation in the results, the heat sink compound was not changed between tests. On inspection of the test data, it did at first appear that the temperature drop and heat flow across the interface were approximately linearly proportional to the temperature differential across the test fixture. However, on plotting the results, as shown in **figure 6.10**, it is apparent that the conductance is not constant. In this figure the results of the last two tests are plotted along with the results of the first test series at the same pressure. The test with the 20 °C differential shows the most variation in both temperature drop and contact conductance with temperature. This test had new interface material at the start of the test. The test with a 40 °C differential shows very nearly the same temperature drop as the original test, but has a consistently higher conductance. As this test used the same interface material as the previous test, it is possible the silicone grease underwent some property change during the first test, possibly due to the more volatile components boiling off. One foreseeable problem with putting too much weight on the results of this particular test series arises from the definition of the contact conductance. It is defined as the heat flux divided by the temperature drop across the interface. But for this test series the heat flux is relatively large and the temperature drop is quite small, so even a minor variation in the temperature drop can result in a large variation in the conductance. It is evident that more testing needs to be done in this area to accurately quantify what processes are occurring.

At the conclusion of the previous test series it was decided that the heat flux sensors might need to be re-calibrated for each temperature span across the test fixture. When calibration tests were performed at a test fixture delta-T of 20 and 40 °C, the results were found to be similar to but not identical with the calibration at a delta-T of 30 °C. With these new calibration constants the previous tests were repeated, with the results shown in **figure 6.11**. As in the previous tests it was apparent that the conductance was not a constant. However it is worth noting again that this derived value is very sensitive to any change in the temperature drop, and that any such error could overwhelm any true trend in the data.

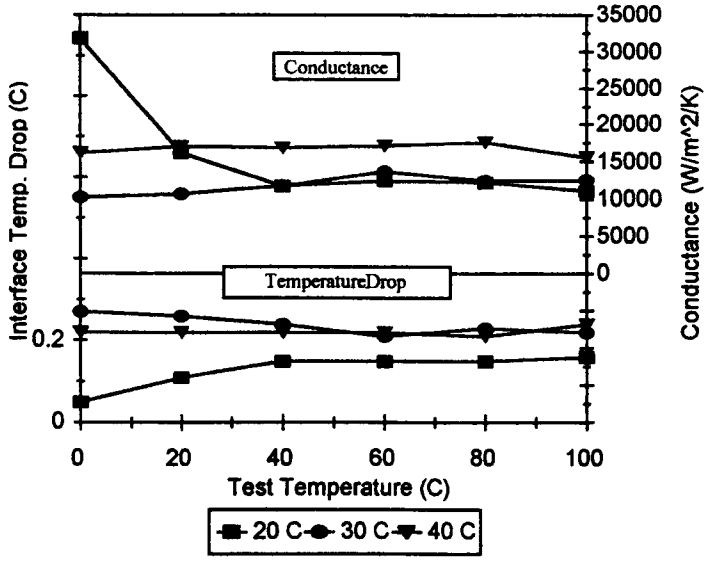

Figure 6.10 Interface conductance and temperature drop with heat sink compound at interface.

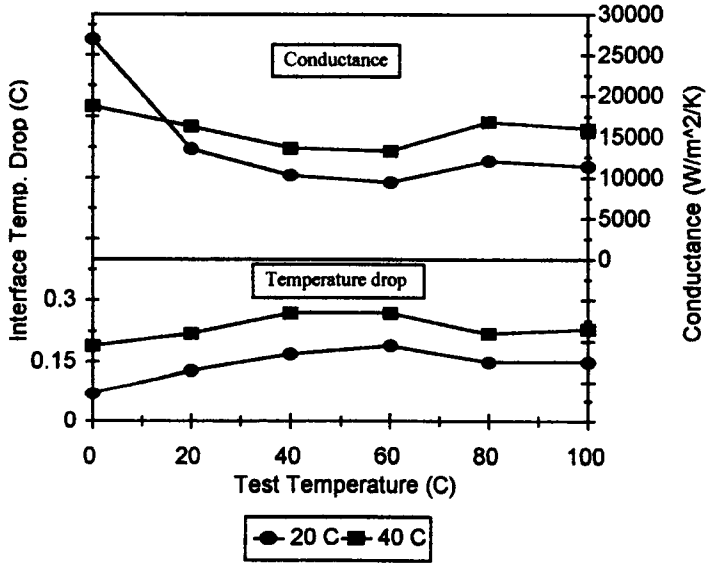

Figure 6.11 Interface conductance and temperature drop with heat sink compound at interface using new calibration constants.

Teflon Tape With Delta-T of 20°C and 40°C

Teflon tape was chosen for re-testing based on the consistent results from the first test series with the same material. This test series was similar to the previous tests in that the temperature differential across the stack was 20 °C and 40 °C. The load was maintained at 100 lb. In order to avoid introducing any unnecessary changes into this test, the Teflon tape was not changed between tests, so that there would be no changes in the interface contact. The results of this test series are shown in **figure 6.12**. The interface temperature drop is roughly proportional to the fixture delta T, that is, the temperature drop with a 40 °C delta T is about twice the temperature drop with a 20 °C delta-T. The conductance again shows an unusual trend in that at the lower end of the test range the two values are considerably different. However, in the upper half of the test range the conductance values are nearly identical. Inspection of the data shows that the heat flux remains nearly constant over the test range for both of the tests, but the temperature drop at the interface is somewhat inconsistent, particularly for the 20 °C test. This reinforces the sensitivity of these calculations to the temperature drop.

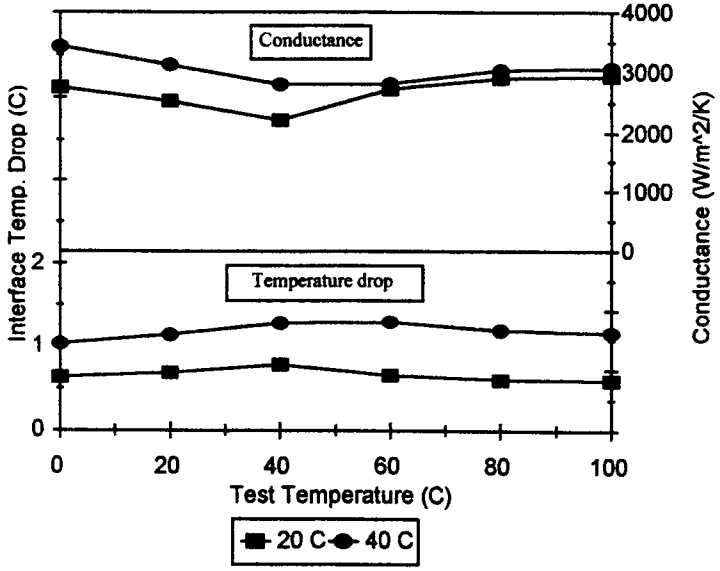

Figure 6.12 Conductance and temperature drop with Teflon tape at interface.

Tabulated Results

Table 6.1 lists the extrapolated surface temperatures, interface temperature differences and the thermal contact conductances (TCC) for average sample temperatures of 0°C and 100°C. In general the results follow the trend of increasing conductance with increasing temperature and pressure. A few of the results don't follow this trend and are most likely in error due to errors in measuring the temperature profile.

The Teflon tape, indium foil and copper foil show the most increase in conductance with increasing pressure, while the heat sink compound and silver paint show little of this tendency. Most of the samples show some increase in conductance with increasing temperature, although this trend is not consistent in all of the samples. It is possible that some trends may be masked by the noise or uncertainty in the system.

Table 6.1 Experimental results for average sample temperatures of 0°C and 100°C with a 30°C fixture temperature difference.

		0°C Average Temperature				100°C Average Temperature			
Interface Material	Load Lbs.	Th °C	Tl °C	DeltaT °C	TCC W/m^2/K	Th °C	Tl °C	DeltaT °C	TCC W/m^2/
None (Air)	50	-0.85	-1.85	1	2696	98.88	97.89	0.994	2727
	200	-0.58	-1.61	1.03	2607	99.11	98.2	0.916	3007
Indium Foil	*25	-0.57	-1.64	1.07	2533	99.04	98.1	0.943	2891
	**50	-0.88	-1.9	1.02	2659	99.06	98.21	0.852	3205
	**100	-0.58	-1.6	1.02	2643	99.1	98.21	0.894	3080
	**250	-0.64	-1.49	0.85	3174	99.03	98.23	0.793	3489
Teflon Tape	*25	0.16	-2.01	2.18	1176	99.03	97.65	1.381	1901
	*50	-.049	-2.20	1.71	1532	99.05	97.82	1.231	2188
	*100	-0.61	-1.07	0.46	5799	98.95	98.48	0.464	5886
	*250	-0.66	-1.03	0.37	7489	98.75	98.33	0.415	6617
Heat Sink Compound	*25	-0.77	-0.86	0.14	19837	98.38	98.14	0.248	11026
	*50	-0.57	-0.83	0.27	10253	98.59	98.37	0.221	12574
	*250	-0.66	-0.84	0.18	15683	98.49	98.35	0.141	19717
Silver Paint	*25	-0.79	-1.04	0.25	11014	98.46	98.19	0.271	10213
	*50	-1.19	-1.45	0.26	10618	98.51	98.49	0.021	13845
	*100	-0.96	-1.28	0.32	8771	98.43	98.26	0.175	15765
	*250	-0.78	-0.95	0.17	16352	98.44	98.23	0.205	13645
Copper Foil	*25	-0.48	-2.18	1.7	1572	98.92	97.58	1.341	1975
	**50	-0.39	-2.00	1.63	1628	98.88	97.62	1.262	2131
	**100	0.01	-1.46	1.47	1835	98.84	97.71	1.131	2393
	**250	0.06	-1.25	1.31	2102	98.76	97.77	0.994	2736
	*250	-0.08	-1.21	1.12	2649	98.99	98.13	0.88	3197

*new interface material **interface material from previous test

7 EXAMINATION OF RADIANT HEAT TRANSFER

A number of references have noted that radiant energy transfer is small enough to be neglected (5,6). To gain some idea of the validity of this assumption, a trial calculation based on typical experimental conditions was performed. The equation for radiant transfer is:

$$\frac{Q}{A} = F * \varepsilon * \sigma * (T_1^4 - T_2^4) \qquad (7.1)$$

where:

	Q/A	heat flow per unit area, (W/m^2);
	F	view factor, ($0<F<1$);
	ε	emissivity, ($0<\varepsilon<1$);
	σ	Stefan-Boltzmann constant, ($5.67*10^{-8} W/m^2/K^4$);
	T_1, T_2	opposing body temperatures, (K).

Taking a typical test, with the split sample, no interface material, 50 lb. load and an average sample temperature of ≈100°C, the total heat transfer was ≈2700 W/m^2, and the upper and lower interface temperatures were 98.88 °C (372.03 K) and 97.89 °C (371.04 K), respectively. For two parallel (infinite) plates in close proximity, we can take the view factor to be ≈1 (10). The emissivity for stainless steel ranges from ≈0.074 for a polished surface, to ≈0.9 for a furnace oxidized surface (11). As the specimens had been sanded on a fine (600 grit) paper, we will estimate the emissivity as 0.1.

Using the above parameters, the contribution from radiation is ≈1.151 W/m^2. If we assume a worst case emissivity of ≈0.9, the contribution is ≈10.36 W/m^2. In the first case, based on a total energy transfer of 2700 W/m^2, this amounts to 0.043 % of the total heat transfer. In the second case it amounts to 0.38 % of the total transfer. Based on the results of these calculations, it should be safe to assume the effects of radiation are negligible.

8 MATHEMATICAL MODEL

An existing analytical model was used to predict the same contact conductance as measured in this work. Veziroglu has formulated a theoretical model to estimate contact conductance by correlating the data from a wealth of experimental results available in the literature (13). These relationships are based on contact or surface parameters, in addition to thermal properties of the contact materials and interstitial fluids. The data from which these correlations were derived was based on conductance tests using various combinations of stainless steel and aluminum contact surfaces, with contact pressures of 5 to 425 psi, RMS surface roughness of 10 to 120 μin and air, brass shim stock or asbestos sheets as interface materials (14). The following nomenclature describes the variables used in this method:

A	interface area	a	accommodation coefficient
B	gap number	C	constriction number
E	emissivity	K	conductivity number
k	thermal conductivity	L_m	mean free path of gas molecules
M	Meyer hardness	m	slope of line
Pr	Prandtl number	p	contact pressure
R_e	contact element radius	S	interface size number
T	absolute temperature	U	conductance number
u	contact conductance/area	δ	effective distance between surfaces
δ_i	surface roughness	γ	ratio of specific heats
ρ	density	σ	Stefan-Boltzmann constant
ν	kinematic viscosity	v	mean molecular velocity

Subscripts:

o	fluid, zero contact pressure	1	solid 1, surface 1
2	solid 2, surface 2	c	actual contact spot
f	equivalent fluid	m	arithmetic mean

The following steps are used for this method. The effective gap thickness (δ) is defined as the sum of the oppposing surface finishes ($\delta_1+\delta_2$) multiplied by a constant:

$$\delta = 3.56(\delta_1 + \delta_2) \qquad (8.1a)$$

$$\delta = 0.46(\delta_1 + \delta_2) \qquad (8.1b)$$

where eq. 8.1a is used if $(\delta_1+\delta_2) < 7.0$ μm and eq. 8.1b is used if $(\delta_1+\delta_2) > 7.0$ μm. The coefficients are the slope of a "best" fit line through the empirical data points of the sum of surface roughness versus the effective gap thickness.

The effective fluid thermal conductivity is determined by:

$$k_f = k_o \tag{8.2a}$$

$$k_f = \frac{k_o}{1+\frac{8\gamma(\frac{\nu}{v})(a_1+a_2-a_1a_2)}{\delta \mathrm{Pr}\, a_1a_2(\gamma+1)}} + \frac{4\sigma\delta E_1E_2T_m^{\,2}}{E_1+E_2-E_1E_2} \tag{8.2b}$$

where eq. 8.2a is used if the interstitial fluid is a liquid, and eq. 8.2b is used if it is a gas.

With the fluid conductivity calculated the conductivity number is found from:

$$K = k_f \frac{k_1+k_2}{2k_1k_2} \tag{8.3}$$

where the individual conductivities are calculated at the arithmetic mean temperature of the respective surface temperatures and the actual contact spots, defined as:

$$T_c = \frac{k_1T_1+k_2T_2}{k_1+k_2} \tag{8.4}$$

The constriction number is defined as the square root of the contact pressure divided by the Meyer hardness:

$$C = \sqrt{\frac{p}{M}} \tag{8.5}$$

The interface size number is the square root of the contact area divided by the effective gap thickness:

$$S = \frac{\sqrt{A}}{\delta} \tag{8.6}$$

The gap number, B, is the relationship between the constriction number and the interface size number, and is applicable to any contact material and surface finish from which these correlations were derived:

$$B = 0.335C^{0.315}S^{0.137} \tag{8.7}$$

where the exponential coefficients were derived by fitting a line to the correlation data.

The conductance number can be found by iteration of the following transcendental equation:

$$U = 1 + \frac{BC}{K\tan^{-1}((1/C)\sqrt{1-(1/U)}-1)} \qquad (8.8)$$

or graphically from **figure 8.1** using C and B/K.

The conductance per unit area can then be calculated as:

$$u = U\frac{k_f}{\delta} \qquad (8.9)$$

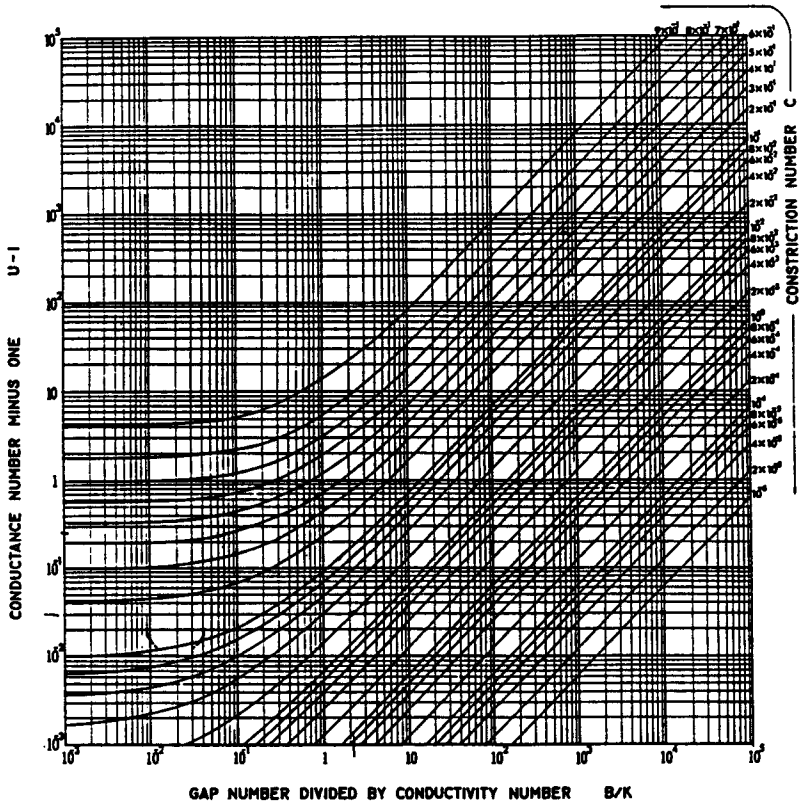

Figure 8.1 Chart for calculating thermal contact conductance (13).

For comparative purposes this model was applied to a stainless steel pair of contact surfaces in air, with no other interface material, with a load of 50 lbs. (160 psi) and an average temperature of 100°C. From testing, a contact conductance of about 2700 W/m^2/K was measured. The theory however predicted a conductance value of about 35000 W/m^2/K, nearly an order of magnitude higher than measured.

Based on examination of the various correlation expressions, it was felt that the most likely cause of this discrepancy was in the derived expressions for the effective gap thickness, equations 8.1a and 8.1b. The coefficients in these two equations are the slopes of a best fit line through the data sets, which have a great deal of scatter, as seen in **figures 8.2** and **8.3**. These correlations are based on a roughness sum of about 0.5 μm to 90 μm. The measured surface roughness of the stainless steel test pieces used in testing for this thesis totaled about 0.14 μm, which is significantly smoother than the data used to formulate the correlations. Inspection of **figure 8.2** shows that there is a distinct group of data points at the low end of the surface roughness scale, which have a nearly vertical alignment. A line drawn through this subset of points would have a slope substantially

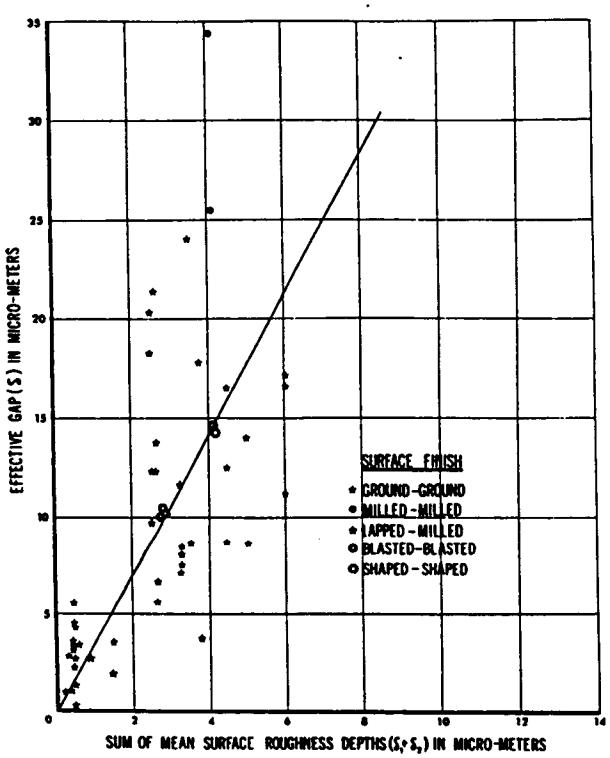

Figure 8.2 Effective gap vs sum of surface roughness for $(\delta_1+\delta_2) < 7\mu m$ (13).

greater than the 3.56 predicted for the set as a whole. It is believed that this distinct trend for relatively smooth contact surfaces is caused by the macro-roughness, or waviness of

the surface. As the surfaces get smoother, the waviness supersedes the micro-roughness as the dominant factor controlling the effective gap thickness. It was theorized that a different method should be employed to correlate the surface roughness to the effective gap thickness for very smooth contact surfaces.

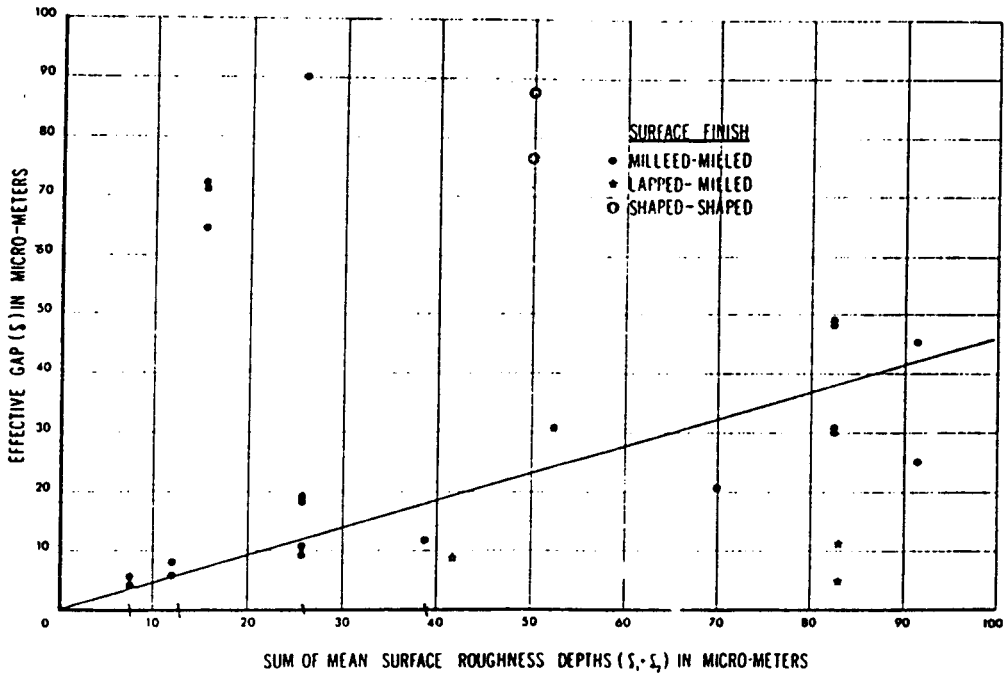

Figure 8.3 Effective gap vs sum of surface roughness for $(\delta_1+\delta_2) > 7\mu m$ (13).

In order for the theoretical conductance to match the measured conductance, the coefficient in equation 1 would need to be approximately 90. A simple linear regression was performed on only the data points with a roughness sum of less than 0.7 μm. The slope of the best fit line through these points was about 42.5, although this line was not forced through the origin, as was done with the mathematical model. If 42.5 was used in the effective gap thickness equation (eq. 1), the model predicted a contact conductance of about 5250 W/m^2/K, which is still nearly twice the measured value.

It was felt that a simple linear regression did not adequately describe the trend in the data sets. The log of the data points was taken and a linear regression performed on

the converted data. This converted data is shown in **figure 8.4** along with the best fit line. When the equation for this line is converted back to non-log form the expression for the effective gap thickness becomes:

$$\delta_{eff} = \frac{\delta_T^{0.478}}{10^{2.462}} \qquad (8.10)$$

where δ_{eff} and δ_T are given in meters. When equation 8.10 is substituted for equation 8.1 in the mathematical model the predicted conductance is14777 W/m^2/K. While this is an improvement on the original effort it is still over 5 times the measured conductance.

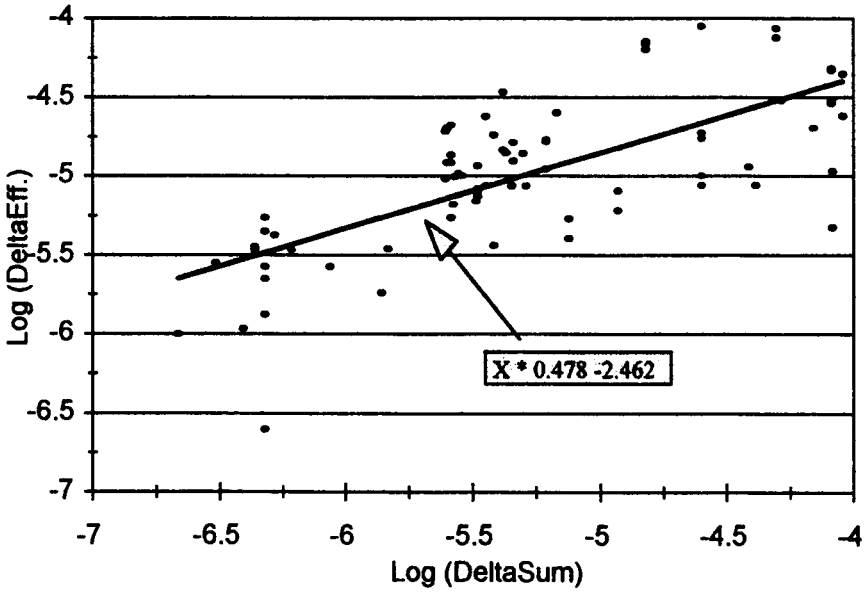

Figure 8.4 Log(δ_T) versus Log(δ_{eff}) for all data points, including best fit line.

It was noted that if δ_T versus the effective gap coefficient for the rough, moderate and smooth data was graphed on a log-log plot, a straight line could be drawn through the approximate center of each data set. A line drawn vertically from the measured surface roughness, ≈0.14 μm, to this line would correspond to the approximate value of the effective gap coefficient needed for the theoretical and measured contact conductance to match. To test this idea the average δ_T for the three data sets was calculated. The log of

this average and the corresponding gap coefficient was taken and a linear regression done to fit a line through these points, as shown in **figure 8.5**. When converted back to non-log form this resulted in the following expression for the effective gap coefficient (EGC):

$$EGC = 10^{1.213} * \delta_T^{-0.969} \qquad (8.11)$$

where δ_T is in microns. Given the total measured roughness of 0.1416 μm, equation 8.11 predicts an effective gap coefficient of 108. When the results of equation 8.11 are substituted into equation 8.1 for the gap coefficient the mathematical model predicts a conductance of 2286 W/m^2/K. This result is less than 17% smaller than the measured conductance. Due to the large degree of scatter in the data sets an exact solution is not probable. But it would appear that several of the preceding methods can be used to improve the approximation of the effective gap thickness for smooth contacts. In particular equation 8.11 improved the estimated conductance for very smooth contacts.

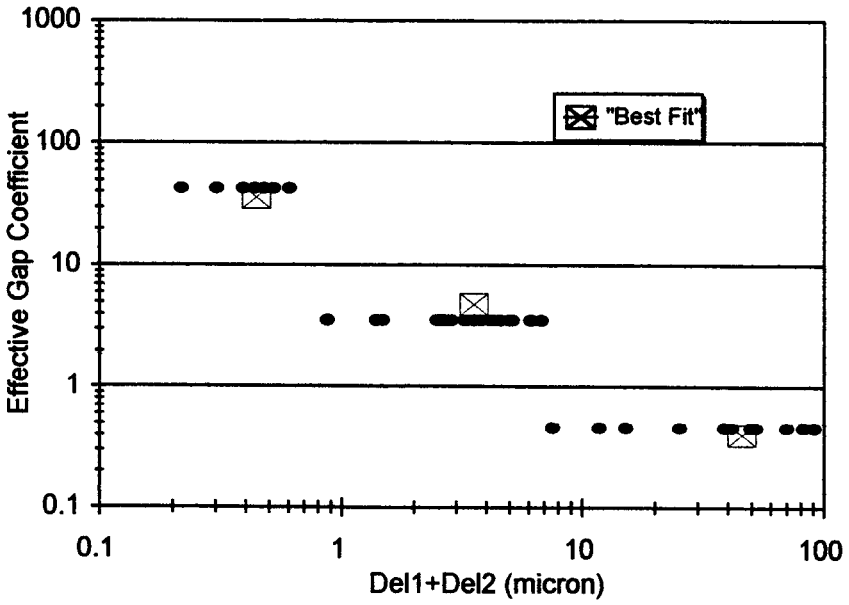

Figure 8.5 Best fit line through smooth, moderate and rough data points.

To use this mathematical model the mechanical and thermo-physical properties of the contact surfaces and interface material must be known, as well as the surface

roughness and contact area and pressure. The equations have been arranged in the order in which they were used to estimate the contact conductance. For very smooth contact surfaces ($(\delta_1+\delta_2) < .5\mu m$), equation 8.11 should be substituted for equation 1. The mean molecular velocity (12) in equation 8.2b was found with the following expression:

$$\upsilon = \sqrt{\frac{8RT}{\pi M}} \qquad (8.12)$$

where:
- R universal gas constant
- T absolute temperature
- M molar mass

The conductance number, U, can be found from equation 8.8 or read from **figure 8.1**. The contact conductance per unit area is than found from equation 8.9.

If a solid interface material, such as copper or indium foil is used this method can be modified by treating the interface as two interfaces (steel to foil + foil to steel) plus the resistance through the foil (15). The total interface temperature drop is then:

$$\Delta T = 2 * \Delta T(steel - foil) + Qt / k \qquad (8.13)$$

where the last term is the thermal resistance due to the thickness of the foil.

9 UNCERTAINTY ANALYSIS

There is a degree of uncertainty in all of the measured and published parameters used in the calculations in this thesis. The uncertainty analysis will be based on the statistical method:

$$\omega R = [(\frac{\partial R}{\partial x_1} * \omega x_1)^2 + (\frac{\partial R}{\partial x_2} * \omega x_2)^2 + \ldots + (\frac{\partial R}{\partial x_n} * \omega x_n)^2]^{\frac{1}{2}} \qquad (9.1)$$

where: ω is the uncertainty in any variable
R is the derived result
x_i is any independent variable
n is the total number of independent variables

The following uncertainty values are based on suppliers specifications, observations or estimates:

T_i	thermocouple output	± 0.05 °C
c_i	flux sensor output	± 2.0 % of reading
v_i	data acquisition system voltage	± 0.05 % of reading
K	NIST sample conductivity	± 5.0 % of published value
$dx_{1,4}$	thermocouples spacing	± 0.015 in.
$dx_{2,3}$	thermocouple to interface distance	± 0.0105 in.

The uncertainty in T_i is based on the observed noise or short term fluctuation in the thermocouple reading. This was thought to be the best estimate of the uncertainty in the thermocouple, as the temperature difference between adjacent thermocouples was the desired quantity, not the absolute temperature. The data system suppliers estimate of an absolute error of ± 0.7 °C would have implied too great an error. The uncertainties in c_i, v_i and K were supplied by the manufacturers. The uncertainties in dx_1 and dx_4 were based on placing a thermocouple tip in an over-sized hole. The holes were 0.021 inch dia. and the thermocouple tip was estimated to be 0.006 inch dia.. This allows ±0.0075 inch variation in placement within the hole, or ±0.015 inch variation between thermocouple pairs. The uncertainty in dx_2 and dx_3 is the sum of the thermocouple placement variation and the estimated uncertainty of 0.003 inch in the distance between the hole and the interface. The thermocouple holes were located with a digital position display on a vertical milling machine, and are considered to be exact for the purpose of this analysis.

The equation for the interface temperature drop is given by:

$$\Delta T = \{T_2 - (\frac{T_1 - T_2}{dx_1})dx_2\} - \{T_3 + (\frac{T_3 - T_4}{dx_4})dx_3\} \qquad (9.2)$$

The equation for the heat flow is given by:

$$Q = Q_{ave}(T_{ave} * C_1 + C_2) \qquad (9.3)$$

where Q_{ave} is given by:

$$Q_{ave} = \frac{V_1 C_1 + V_2 C_2}{2} \qquad (9.4)$$

and the term: $(T_{ave}*C_1+C_2)$ is a temperature correction factor derived by performing a linear regression with Q_{ave} being the dependent variable and Q_{NIST} being the independent variable (see calibration section for details). Q_{NIST} is given by:

$$Q_{NIST} = K(\frac{T_1 - T_2}{dx}) \qquad (9.5)$$

where:	K=K(T)	NIST SRM thermal conductivity
	T_1, T_2	thermocouple temperatures
	dx	distance between thermocouples

The uncertainty in equation 9.3 is a function of the uncertainty in equation 9.4 and the uncertainty in the temperature correction factor, which will be considered the same as the uncertainty in equation 9.5. Based on data from a typical calibration test, the uncertainty in equation 9.5 was found to average 5.3 %. The thermal contact conductance is then given by:

$$TCC = \frac{Q}{\Delta T} \qquad (9.6)$$

The uncertainty in the measured and derived results can then be determined by the application of equation 9.1 to the appropriate equations.

Using the methods outlined above, the uncertainties for the interface temperature drop, heat flux and thermal contact conductance for a representative selection of experiments were calculated. The uncertainty for the heat flux remained constant at about 5.5 % for all the experiments. The uncertainty in the thermal contact conductance ranged from about 7.5 % in the experiment using Teflon tape with a load of 25 lbs. at an average temperature of 0°C to 80.9 % in the experiment using heat sink compound with a load of 250 lbs. at an average temperature of 100 °C. As can be seen in **Table 9.1**, the

uncertainty in the thermal contact conductance is in all cases slightly higher than the uncertainty in the interface temperature drop, while the heat flow uncertainty remains constant. This is because the uncertainty in the interface temperature drop is the dominant factor and has a greater influence than the other factors.

Table 9.1 Uncertainty calculations for selected experiments.

Parameters			Uncertainty		
Interface Material	Load (lbs.)	Temperature (°C)	Interface Temperature Drop (%)	Heat Flux (%)	Contact Conductance (%)
None	50	0	11.45	5.49	12.7
None	50	100	11.0	5.49	12.3
Heat Sink Compound	250	0	67.53	5.48	67.75
Heat Sink Compound	250	100	80.7	5.48	80.9
Teflon Tape	25	0	5.18	5.49	7.55
Teflon Tape	25	100	7.62	5.49	9.39
Teflon Tape	250	0	33.47	5.49	33.91
Teflon Tape	250	100	27.93	5.49	28.47

10 CONCLUSIONS

Interface materials and interface pressure have been examined with the aid of a thermal conductivity test fixture. Both factors have been found to influence the interface contact conductance and resulting interface temperature drop. The materials were tested at the interface of identical pieces fabricated from stainless steel. Clamping loads ranged from 25 pounds to 250 pounds, being limited by the compression strength of the heat flux sensors. The tests were conducted over a temperature range of 0 °C to 100 °C in increments of 20 °C. The temperature differential across the test fixture was either 20 °C, 30 °C or 40 °C. Interface materials included air, silicone based heat sink compound, Teflon tape, silver filled paint, indium foil and annealed copper foil. In addition, surface roughness affects the contact conductance, and is a necessary input parameter to estimate the contact conductance using a mathematical model.

The ability of the interface material to conform to the surface of the opposing materials appears to be a greater factor than the conductivity of the material. It was found that a silicone based heat sink compound and a silver filled paint most improved the conductance, while metallic foils such as indium and annealed copper either didn't affect or reduced the contact conductance, as indicated by an increase in interface temperature drop compared to the tests using no interface material.

The ability of the heat sink compound and the silver paint to conduct energy at the interface was independent of the applied load. The Teflon tape showed increasing conductance with increasing load up to 100 pounds, but little improvement when the load was increased to 250 pounds. Both the indium foil and annealed copper foil showed an increase in conductance as the load was increased, with no indication that a limit had been reached within this load range.

The conductance of most of the materials tested appeared to have some dependence on the test temperature. This trend is most apparent in the copper and indium foils and the Teflon tape at lower pressures. Inspection of the graphs of the temperature drops for these materials shows that the conductance increases as the test temperature

increases. There also appears to be some interdependence with the flow stress of the material. The silicone grease and silver paint showed no dependence on either the test temperature or the pressure. The Teflon tape conductance showed a dependence on temperature at lower pressures, but none above the loading at which the flow stress had apparently been exceeded. The metallic foil conductances increased with temperature at all pressure loading. Perhaps if the flow stress of the foils had been reached the conductance would have been unaffected by the test temperature. The conductivity of most materials increases with temperature, but not by the amount indicated by the test results.

An effort was made to determine if the contact conductance was constant for a given interface situation by changing the fixture temperature differential, with a proportional change in heat flux. It was found that both the interface temperature drop and heat flow were approximately proportional to the temperature differential, as would be expected, but the conductance did not appear to remain constant. However, careful selection of the test parameters, with careful control of the test conditions might yield better results. It was felt that the conductance values could have been unduly affected by the cumulative effect of the system errors.

The contact conductance of an air filled interface was estimated with the use of a mathematical model formulated by Veziroglu (13). This model was found to over-estimate the conductance by an order of magnitude. Investigation of the variables showed that the results were most heavily influenced by the effective gap thickness (eq's 1a & 1b). Apparently the mathematical model fails to accurately predict the effective gap thickness for very smooth contact surfaces (< 0.5 μm). A new expression was formulated that when incorporated into the model produced an estimated conductance that was within 17 % of the measured value for an air gap. This expression:

$$EGC = 10^{1.213} * \delta_T^{-0.969} \qquad (11)$$

is used to compute the numerical constants in eq. 1 in the mathematical model. Although it has not been tested for rougher contact surfaces, this expression was derived from data for a wide range of surface roughness values and should be equally applicable to other surface conditions.

It is evident from the literature review and also from the experimental results that contact conductance is a complex mechanism. Perhaps the most difficult parameter to accurately quantify is the actual contact area, which is heavily influenced by the surface factors, including both roughness and waviness, as well as the hardness of the material. There is room for much more testing and analysis on this subject.

11 SUGGESTIONS FOR FURTHER RESEARCH

These series of tests were limited by certain characteristics of the test apparatus. The maximum pressure had to be kept below ≈2000 psi to protect the heat flow sensors. At the pressures and loads tested there were certain trends evident in the conductance values. With the silicone grease, Teflon tape and silver paint it appeared that increasing the pressure would have no further effect on the conductance. But with the harder materials, i.e. indium foil and copper foil, the trend to increased conductance with increasing pressure had evidently not reached a maximum.

The temperature was limited by the solder in the text fixture, and the insulation as well. Most of the graphs of the harder materials seemed to indicate that the conductance continued to change with the test temperature, even up to the maximum temperature, perhaps because of the temperature dependency of the conductivity and flow stress.

All the tests were done with the surface prepared in a single way, by sanding with 600 grit sandpaper. This resulted in a distinct directional orientation to the surface asperities, which could have resulted in a dependence on the relationship between the two opposing surfaces. The literature suggests that the surface roughness, in conjunction with pressure and interface material, can significantly affect the contact conductance. In particular, the method used to prepare the surfaces of the test specimens, and the orientation of the test pieces, could have resulted in an artificially low true contact area. Further testing could be done to measure the impact of the surface finish and orientation.

In general the results of the preceding research efforts show a fair degree of scatter and inconsistency. Further testing could possibly verify or disprove some of the findings and trends. Careful attention should be given to the surface preparation and flatness in particular. As all of the testing was done with the same stainless steel test pieces the results are limited to applications involving the same materials.

BIBLIOGRAPHY

1 Pike, J.N., J.F. Doar, *High Temperature Thermal Conductivity Measurements. Theory of Longmire's Method and the Rectangular Bar Method.* Union Carbide Corporation, URM-25, 1960.

2 ASTM designation C-177-85. *Standard Test Method for Steady-State Heat Flux Measurements and Thermal Transmission Properties by Means of the Guarded-Hot-Plate Apparatus.* American Society of Testing and Materials. 1991.

3 ASTM designation C-518-91. *Standard Test Method for Steady-State Heat Flux Measurements and Thermal Transmission Properties by Means of the Heat Flow Meter Apparatus.* American Society of Testing and Materials. 1991.

4 Ashworth, T., E. Ashworth, S. F. Ashworth. *Thermal Conductivity 21: A New Apparatus for Use With Materials of Intermediate Conductivity.* New York: Plenum Press. 1990.

5 Giommi, M., M. Marchetti, P. Testa, F.R. Torrisi, *Measurement of Thermal Conductivity and Thermal Contact Resistance in Composite Materials for Space Applications.* ICCM-VI.

6 Hsieh, C. K., Y. S. Touloukian. *Correlation and Prediction of Thermal Contact Conductance for Nominally Flat Surfaces, 8th Conference on Thermal Conductivity.* Plenum Press. 1968.

7 Rohsenow, W. M., *Handbook of Heat Transfer.* New York: McGraw-Hill. 1973.

8 McWaid, T., E. Marschall, *Thermal Contact Resistance Across Pressed Metal Contacts in a Vacuum Environment, Int. J Heat Mass Transfer.* Vol. 35. Great Britain. 1992.

9 Ochterbeck, J. M., G. P. Peterson, L. S. Fletcher, *Thermal Contact Conductance of Metallic Coated BiCaSrCuO Superconductor/Copper Interfaces at Cryogenic Temperatures, ASME/JSME Thermal Engineering Proceedings.* Vol. 1, 1991.

10 Guyer, E. C.. *Handbook of Applied Thermal Design*, New York, McGraw-Hill. 1989.

11 Welty, J. R., C. E. Wicks, R, E. Wilson, *Fundamentals of Momentum, Heat and Mass Transfer*, 3rd Ed., New York, John Wiley and Sons. 1984.

12 Atkins, P., *Physical Chemistry, 5th Ed.*, 1994, New York, W. H. Freeman and Co.

13 Veziroglu, T. N., *Correlation of Thermal Contact Conductance Experimental Results, Progress in Astronautics and Aeronautics, Vol. 20*, Academic Press, New York, 1967.

14 Barzelay, M.E, K.N. Tong, G.F. Holloway, *Effect of Pressure on Thermal Conductance of Contact Joints, Technical Note 3295, National Advisory Committee for Aeronautics*, Washington, 1955.

15 Wolff, E. G., Schneider, D. A., *Prediction of Thermal Contact Resistance Between Polished Surfaces, International Journal of Heat and Mass Transfer*, 1998.